J|A|C|S
ARTICLES
Published on Web 02/24/2007

Photoinitiated Charge Transport in Supramolecular Assemblies of a 1,7,*N,N′*-Tetrakis(zinc porphyrin)-perylene-3,4:9,10-bis(dicarboximide)

Richard F. Kelley, Won Suk Shin, Boris Rybtchinski, Louise E. Sinks, and Michael R. Wasielewski*

Contribution from the Department of Chemistry and International Institute for Nanotechnology, Northwestern University, Evanston, Illinois 60208-3113

Received September 7, 2006; E-mail: m-wasielewski@northwestern.edu

Abstract: We report the synthesis and photophysical characterization of a multichromophore array, $(Z3PN)_4PDI$, consisting of four zinc 5-phenyl-10,15,20-tri(*n*-pentyl)porphyrins (Z3PN) attached to the 1,7,*N,N′*-positions of perylene-3,4:9,10-bis(dicarboximide) (PDI). The dynamics of energy and charge transport within this system were compared to those of two model compounds, *N,N′*-$(Z3PN)_2PDI$ and 1,7-$(Z3PN)_2PDI$. The symmetry of the lowest unoccupied and highest occupied molecular orbitals of PDI results in significantly different electronic couplings between Z3PN and PDI when they are connected at the 1,7-positions vs the *N,N′*-positions of PDI. This results in two distinct pathways for electron transfer in $(Z3PN)_4PDI$. Using a combination of metal−ligand binding with the bidentate ligand 1,4-diazabicyclo[2.2.2.]-octane (DABCO) and $\pi-\pi$ stacking, $(Z3PN_4)PDI$ forms a supramolecular assembly, $[[(Z3PN)_4PDI]_2-DABCO_4]_2$, in toluene solution. The structure of this hierarchical assembly is characterized with the use of solution-phase X-ray scattering techniques and demonstrates both efficient light harvesting and facile charge separation and transport using multiple pathways.

Introduction

Well-ordered assemblies of photofunctional chromophores are responsible for the efficient energy and electron transfer found in photosynthetic light-harvesting and reaction center proteins.[1−5] Natural photosynthetic systems make repetitive use of chlorophyll molecules having different environments determined by the surrounding protein to promote directional energy or electron transfer. In a similar fashion, organization of chromophores into ordered structures is critical to the development of advanced photonic materials designed to carry out complex energy- and electron-transport functions.[6−8] Self-assembly of relatively simple molecular modules into large supramolecular structures using noncovalent interactions is one of the most promising strategies for the preparation of photofunctional materials.[6,8−31] The properties of the covalent units frequently define a self-assembly pattern, which in turn determines the function of the

(1) McDermott, G.; Prince, S. M.; Freer, A. A.; Hawthornthwaite-Lawless, A. M.; Papiz, M. Z.; Cogdell, R. J.; Isaacs, N. W. *Nature* **1995**, *374*, 517−521.
(2) McLuskey, K.; Prince, S. M.; Cogdell, R. J.; Isaacs, N. W. *Biochemistry* **2001**, *40*, 8783−8878.
(3) Pullerits, T.; Sundström, V. *Acc. Chem. Res.* **1999**, *29*, 381−389.
(4) Savage, H.; Cyrklaff, M.; Montoya, G.; Kuhlbrandt, W.; Sinning, I. *Structure* **1996**, *4*, 243−252.
(5) Walz, T.; Jamieson, S. J.; Bowers, C. M.; Bullough, P. A.; Hunter, C. N. *J. Mol. Biol.* **1998**, *282*, 833−845.
(6) Ikkala, O.; ten Brinke, G. *Science* **2002**, *295*, 2407−2409.
(7) Kim, D.; Osuka, A. *Acc. Chem. Res.* **2004**, *37*, 735−745.
(8) Lehn, J.-M. *Science* **2002**, *295*, 2400−2403.
(9) Reinhoudt, D. N.; Crego-Calama, M. *Science* **2002**, *295*, 2403−2407.
(10) Ahrens, M. J.; Sinks, L. E.; Rybtchinski, B.; Liu, W.; Jones, B. A.; Giaimo, J. M.; Gusev, A. V.; Goshe, A. J.; Tiede, D. M.; Wasielewski, M. R. *J. Am. Chem. Soc.* **2004**, *126*, 8284−8294.
(11) Fuller, M. J.; Sinks, L. E.; Rybtchinski, B.; Giaimo, J. M.; Li, X.; Wasielewski, M. R. *J. Phys. Chem. A* **2005**, *109*, 970−975.
(12) Li, X.; Sinks, L. E.; Rybtchinski, B.; Wasielewski, M. R. *J. Am. Chem. Soc.* **2004**, *126*, 10810−10811.
(13) Rybtchinski, B.; Sinks, L. E.; Wasielewski, M. R. *J. Phys. Chem. A* **2004**, *108*, 7497−7505.
(14) Rybtchinski, B.; Sinks, L. E.; Wasielewski, M. R. *J. Am. Chem. Soc.* **2004**, *126*, 12268−12269.
(15) van der Boom, T.; Hayes, R. T.; Zhao, Y.; Bushard, P. J.; Weiss, E. A.; Wasielewski, M. R. *J. Am. Chem. Soc.* **2002**, *124*, 9582−9590.
(16) Ajayaghosh, A.; George, S. J.; Praveen, V. K. *Angew. Chem., Int. Ed.* **2003**, *42*, 332−335.
(17) Brunsveld, L.; Vekemans, J. A. J. M.; Hirschberg, J. H. K. K.; Sijbesma, R. P.; Meijer, E. W. *Proc. Natl. Acad. Sci. U.S.A.* **2002**, *99*, 4977−4982.
(18) Cheng, X. H.; Diele, S.; Tschierske, C. *Angew. Chem., Int. Ed.* **2000**, *39*, 592−595.
(19) El-Ghayoury, A.; Schenning, A. P. H. J.; van Hal, P. A.; van Duren, J. K. J.; Janssen, R. A. J.; Meijer, E. W. *Angew. Chem., Int. Ed.* **2001**, *40*, 3660−3663.
(20) Engelkamp, H.; Middelbeek, S.; Nolte, R. J. M. *Science* **1999**, *284*, 785−788.
(21) Fenniri, H.; Deng, B.-L.; Ribbe, A. E. *J. Am. Chem. Soc.* **2002**, *124*, 11064−11072.
(22) Gesquiere, A.; Jonkheijm, P.; Hoeben, F. J. M.; Schenning, A. P. H. J.; De Feyter, S.; De Schryver, F. C.; Meijer, E. W. *Nano Lett.* **2004**, *4*, 1175−1179.
(23) van Herrikhuyzen, J.; Syamakumari, A.; Schenning, A. P. H. J.; Meijer, E. W. *J. Am. Chem. Soc.* **2004**, *126*.
(24) Hirschberg, J. H. K. K.; Brunsveld, L.; Ramzi, A.; Vekemans, J. A. J. M.; Sijbesma, R. P.; Meijer, E. W. *Nature* **2000**, *407*, 167−170.
(25) Jonkheijm, P.; Miura, A.; Zdanowska, M.; Hoeben, F. J. M.; Feyter, S. D.; Schenning, A. P. H. J.; Schryver, F. C. D.; Meijer, E. W. *Angew. Chem., Int. Ed.* **2004**, *43*, 74−78.
(26) Kleppinger, R.; Lillya, C. P.; Yang, C. *J. Am. Chem. Soc.* **1997**, *119*, 4097−4102.
(27) Thalacker, C.; Würthner, F. *Adv. Funct. Mater.* **2002**, *12*, 209−218.
(28) Würthner, F.; Thalacker, C.; Sautter, A. *Adv. Mater.* **1999**, *11*, 754−758.
(29) Haycock, R. A.; Hunter, C. A.; James, D. A.; Michelsen, U.; Sutton, L. R. *Org. Lett.* **2000**, *2*, 2435−2438.
(30) Haycock, R. A.; Yartsev, A.; Michelsen, U.; Sundstrom, V.; Hunter, C. A. *Angew. Chem.* **2000**, *39*, 3616−3619.
(31) Mak, C. C.; Bampos, N.; Sanders, J. K. M. *Angew. Chem.* **1998**, *37*, 3020−3023.

self-assembled array. In this hierarchical approach, the symmetry of the molecular building blocks not only controls the geometry of the assemblies formed from these subunits but also the directionality of photoinduced electron transfer.

Perylene-3,4:9,10-bis(dicarboximide) (PDI) chromophores are excellent building blocks for covalent and noncovalent photofunctional arrays.[10−15,23,27,28,32−41] PDI has two distinct sites to which electron donors and/or acceptors can be easily attached: the nitrogen atoms of the imides and the 1,6,7,12-carbon atoms at its long edges. Electronic structure calculations show that both the HOMO and LUMO of PDI have nodal planes that bisect the molecule along the N−N axis, so that the π-electron density in these orbitals is much greater at the 1,6,7,12-carbon atoms than at the imide nitrogen atoms.[42] Rates of electron transfer k_{DA}, are given by $k_{DA} \propto V_{DA}^2$(FCWD), where V_{DA} is the electronic coupling matrix element and FCWD is the Franck−Condon weighted density of states.[43−45] Through-bond Dexter-type energy transfer,[46] when viewed formally as two electron transfers, can also be described using a similar expression involving the product of the electronic coupling matrix elements for each electron transfer.[47,48] Since V_{DA} depends strongly on orbital overlap between the frontier molecular orbital of the donor with that of the acceptor,[49] rates of electron transfer and Dexter-type energy transfer depend strongly on the electron density distributions within these orbitals.[50,51] Thus, attaching identical electron donors to sites on PDI having orbital coefficients that differ greatly should in principle result in large differences in electron-transfer rates, making it possible to tailor the rates of individual electron-transfer pathways in a complex donor−acceptor array.

It is well-known that the rates of both Dexter-type energy transfer and electron transfer to or from metalloporphyrins depend on which position of the macrocycle the donor or acceptor is attached.[50,52−55] The two highest occupied molecular orbitals (HOMO and HOMO−1) within metalloporphyrins are nearly degenerate and have electron density distributions that differ greatly.[56−58] The a_{1u} orbital has significant electron density at the β-carbons of the porphyrin with little density at the meso positions, while the opposite is true for the a_{2u} orbital. The energetic ordering of these two orbitals in the metalloporphyrin depends on the nature and the position of the substituents attached to the porphyrin.[58] Substituting electron-donating groups, e.g., phenyl rings or alkyl chains, at the meso positions (5,10,15,20) of the porphyrin raises the energy of the a_{2u} orbital above that of the a_{1u} orbital, making the a_{2u} orbital the HOMO, while substitution of the β-positions with similar electron-releasing groups results in the a_{1u} orbital being the HOMO.[58,59] Generally, increased electron density at particular peripheral carbon atoms of the porphyrin results in stronger electronic coupling to molecules attached to those positions, and consequently in faster electron-transfer rates.[49] For example, Hayes et al.[53] showed that a zinc porphyrin having a pyromellitimide electron acceptor attached to a *meso*-phenyl group has a charge recombination rate that is 3 times faster than that of a porphyrin in which the acceptor is attached to a β-phenyl group. The intense, complementary electronic spectra of Z3PN and PDI result in absorption of a large portion of the solar spectrum between 400 and 650 nm. It has already been shown that photoinduced electron transfer occurs rapidly and efficiently from ^{1*}Z3PN to PDI derivatives.[60,61] Each of these examples is consistent with dominant through-bond, superexchange-mediated electron transfer.[62−66]

Coordination bond formation using metal centers and polydentate ligands is an attractive strategy for building self-assembled structures in which the geometries of the covalent building blocks dictate the structure of the assemblies. Increasing the number of coordination bonding sites within the structure enhances allosteric effects and increases control over the assembly geometry. Multiporphyrin arrays, in which coordination bonds are formed between bidentate ligands and the porphyrin metal centers, represent an important controllable assembly motif.[67−77] There are many examples of multipor-

(32) Würthner, F. *Chem. Commun.* **2004**, 1564−1579.
(33) Xiao, S.; El-Khouly, M. E.; Li, Y.; Gan, Z.; Liu, H.; Jiang, L.; Araki, Y.; Ito, O.; Zhu, D. *J. Phys. Chem. B* **2005**, *109*, 3658−3667.
(34) Liu, Y.; Wang, N.; Li, Y.; Liu, H.; Li, Y.; Xiao, J.; Xu, X.; Huang, C.; Cui, S.; Zhu, D. *Macromolecules* **2005**, *38*, 4880−4887.
(35) He, X.; Liu, H.; Li, Y.; Liu, Y.; Lu, F.; Li, Y.; Zhu, D. *Macromol. Chem. Phys.* **2005**, *206*, 2199−2205.
(36) You, C.-C.; Würthner, F. *J. Am. Chem. Soc.* **2003**, *125*, 9716−9725.
(37) You, C.-C.; Würthner, F. *Org. Lett.* **2004**, *6*, 2401−2404.
(38) Prodi, A.; Chiorboli, C.; Scandola, F.; Iengo, E.; Alessio, E.; Dobrawa, R.; Würthner, F. *J. Am. Chem. Soc.* **2005**, *127*, 1454−1462.
(39) You, C.-C.; Dobrawa, R.; Saha-Moeller, C. R.; Würthner, F. *Top. Curr. Chem.* **2005**, *258*, 39−82.
(40) Beckers, E. H. A.; Meskers, S. C. J.; Schenning, A. P. H. J.; Chen, Z.; Würthner, F.; Marsal, P.; Beljonne, D.; Cornil, J.; Janssen, R. A. J. *J. Am. Chem. Soc.* **2006**, *128*, 649−657.
(41) An, Z.; Yu, J.; Jones, S. C.; Barlow, S.; Yoo, S.; Domercq, B.; Prins, P.; Siebbeles, L. D. A.; Kippelen, B.; Marder, S. R. *Adv. Mater. (Weinheim)* **2005**, *17*, 2580−2583.
(42) Burquel, A.; Lemaur, V.; Beljonne, D.; Lazzaroni, R.; Cornil, J. *J. Phys. Chem. A* **2006**, *110*, 3447−3453.
(43) Hopfield, J. J. *Proc. Natl. Acad. Sci. U.S.A.* **1974**, *71*, 3640−3644.
(44) Jortner, J. *J. Chem. Phys.* **1976**, *64*, 4860−4867.
(45) Marcus, R. A. *J. Chem. Phys.* **1984**, *81*, 4494−4500.
(46) Dexter, D. L. *J. Chem. Phys.* **1953**, *21*, 836−850.
(47) Closs, G. L.; Johnson, M. D.; Miller, J. R.; Piotrowiak, P. *J. Am. Chem. Soc.* **1989**, *111*, 3751−3753.
(48) Closs, G. L.; Piotrowiak, P.; MacInnis, J. M.; Fleming, G. R. *J. Am. Chem. Soc.* **1988**, *110*, 2652−2653.
(49) Plato, M.; Möbius, K.; Michel-Beyerle, M. E.; Bixon, M.; Jortner, J. *J. Am. Chem. Soc.* **1988**, *110*, 7279−7285.
(50) Holten, D.; Bocian, D. F.; Lindsey, J. S. *Acc. Chem. Res.* **2002**, *35*, 57−69.
(51) Tsai, H.; Simpson, M. C. *Chem. Phys. Lett.* **2002**, *353*, 111−118.
(52) Redmore, N. P.; Rubtsov, I. V.; Therien, M. J. *J. Am. Chem. Soc.* **2003**, *125*, 8769−8778.
(53) Hayes, R. T.; Wasielewski, M. R. *J. Phys. Chem A* **2004**, *108*, 2375−2381.
(54) Strachan, J.-P.; Gentemann, S.; Seth, J.; Kalsbeck, W. A.; Lindsey, J. S.; Holten, D.; Bocian, D. F. *J. Am. Chem. Soc.* **1997**, *119*, 11191−11201.
(55) Osuka, A.; Marumo, S.; Maruyama, K.; Mataga, N.; Tanaka, Y.; Taniguchi, S.; Okada, T.; Yamazaki, I.; Yoshinobu, N. *Bull. Chem. Soc. Jpn.* **1995**, *68*, 262−276.
(56) Gouterman, M. *Porphyrins* **1978**, *3*, 1−165.
(57) Weiss, C.; Kobayashi, H.; Gouterman, M. *J. Mol. Spectrosc.* **1965**, *16*, 415−450.
(58) Fajer, J.; Borg, D. C.; Forman, A.; Dolphin, D.; Felton, R. H. *J. Am. Chem. Soc.* **1970**, *92*, 3451−3459.
(59) Atamian, M.; Wagner, R. W.; Lindsey, J. S.; Bocian, D. F. *Inorg. Chem.* **1988**, *27*, 1510−1512.
(60) Gosztola, D.; Niemczyk, M. P.; Wasielewski, M. R. *J. Am. Chem. Soc.* **1998**, *120*, 5118−5119.
(61) Hayes, R. T.; Wasielewski, M. R.; Gosztola, D. *J. Am. Chem. Soc.* **2000**, *122*, 5563−5567.
(62) Anderson, P. W. *Phys. Rev.* **1950**, *79*, 350−356.
(63) Anderson, P. W. *Phys. Rev.* **1959**, *115*, 2−13.
(64) McConnell, H. M. *J. Chem. Phys.* **1961**, *35*, 508−515.
(65) Marcus, R. A. *Chem. Phys. Lett.* **1987**, *133*, 471.
(66) Ogrodnik, A.; Michel-Beyerle, M. E. *Z. Naturforsch.* **1989**, *44a*, 763−764.
(67) Tabushi, I.; Kugimiya, S.; Kinnaird, M. G.; Sasaki, T. *J. Am. Chem. Soc.* **1985**, *107*, 4192−4199.
(68) Hunter, C. A.; Meah, M. N.; Sanders, J. K. M. *J. Chem. Soc., Chem. Commun.* **1988**, 694−696.
(69) Hunter, C. A.; Leighton, P.; Sanders, J. K. M. *J. Chem. Soc., Perkin Trans. 1* **1989**, 547−552.
(70) Camara-Campos, A.; Hunter, C. A.; Tomas, S. *Proc. Natl. Acad. Sci. U.S.A.* **2006**, *103*, 3034−3038.
(71) Ballester, P.; Oliva, A. I.; Costa, A.; Deya, P. M.; Frontera, A.; Gomila, R. M.; Hunter, C. A. *J. Am. Chem. Soc.* **2006**, *128*, 5560−5569.
(72) Ballester, P.; Costa, A.; Deya, P. M.; Frontera, A.; Gomila, R. M.; Oliva, A. I.; Sanders, J. K. M.; Hunter, C. A. *J. Org. Chem.* **2005**, *70*, 6616−6622.

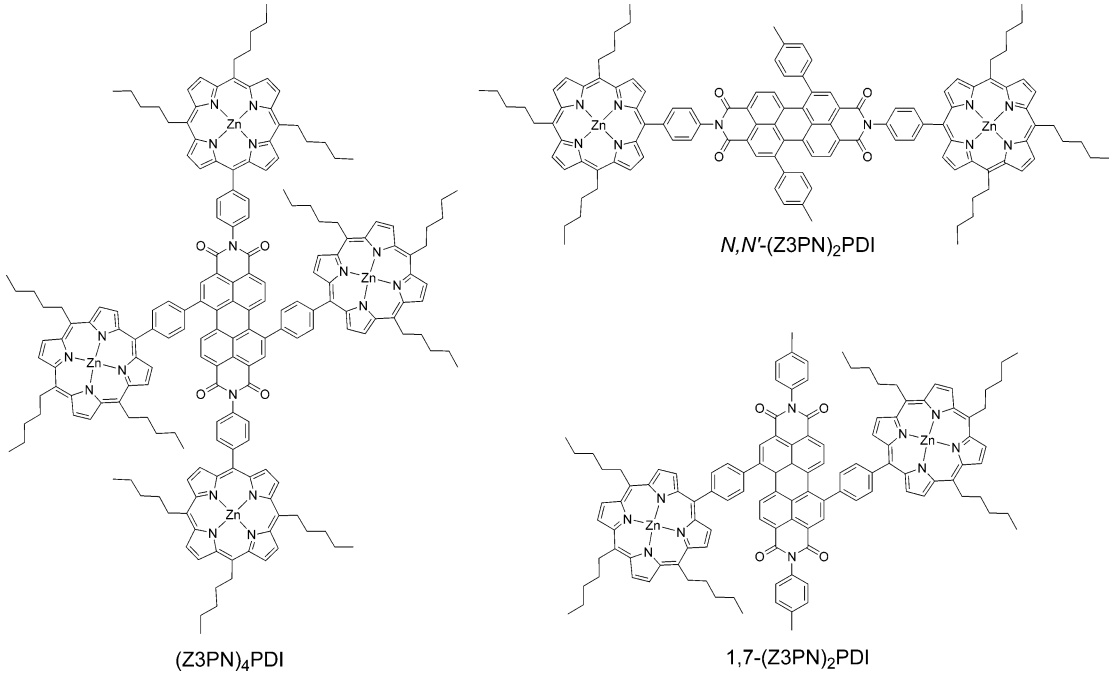

Figure 1. Structures of molecules used in this study.

phyrin systems in which coordination bonds between the bidentate ligand 1,4-diazabicyclo[2.2.2]octane (DABCO) and porphyrin metal centers are used to prepare porphyrin dimers.[31,67,68,71,73,78,79]

There are numerous reports on the self-assembly of both zinc porphyrin and PDI derivatives alone, yet there are relatively few examples in which both of these important donor−acceptor building blocks are incorporated into specific covalent structures to elicit different supramolecular photofunctional assemblies.[15,33,37,38] We reported earlier on supramolecular assemblies in which four PDI derivatives were appended to the para position of each phenyl within zinc *meso*-tetraphenylporphyrin.[15] These molecules formed large, ordered supramolecular assemblies in which the assembly was driven mainly by $\pi-\pi$ interactions of the PDI electron acceptors. Here we report the synthesis and photophysical characterization of a multichromophore array constructed from four zinc 5-phenyl-10,15,20-tri(*n*-pentyl)-porphyrins (Z3PN) attached to the 1,7,*N*,*N*′-positions of PDI to give (Z3PN$_4$)PDI, Figure 1. We also report the dynamics of energy- and charge transport of two model compounds, *N*,*N*′-(Z3PN)$_2$PDI and 1,7-(Z3PN)$_2$PDI, which help to interpret the data obtained from the full array. As mentioned above, the symmetry of the lowest unoccupied molecular orbital of PDI results in significantly different electronic couplings between Z3PN and PDI when they are connected at the 1,7-positions vs the *N*,*N*'-positions of PDI. This results in two distinct pathways for electron transfer in (Z3PN)$_4$PDI. Using a combination of metal−ligand binding with (DABCO) and $\pi-\pi$ stacking, (Z3PN$_4$)PDI forms a supramolecular assembly, [[(Z3PN)$_4$PDI]$_2$−DABCO$_4$]$_2$, in toluene solution. The structure of this assembly is characterized using solution-phase X-ray scattering techniques and demonstrates both efficient light harvesting and facile charge separation and transport using multiple pathways.

Experimental Section

The syntheses and characterization of (Z3PN)$_4$PDI and model compounds, 1,7-(Z3PN)$_2$PDI and *N*,*N*′-(Z3PN)$_2$PDI, Figure 1, are described in detail in the Supporting Information. UV−vis absorption measurements were made with a Shimadzu spectrometer (UV1601). All solvents were reagent grade or better and were purified using standard procedures. Toluene used for spectroscopic and X-ray scattering measurements was purified by passing it through a series of CuO and alumina columns (GlassContour) immediately prior to use. Electrochemical measurements were performed using a CH Instruments model 660A electrochemical workstation. Reversible half-wave potentials were determined in butyronitrile containing 0.1 M *n*-Bu$_4$N$^+$-BF$^-_4$ using a Pt working electrode, a Pt wire counter electrode, a Ag/Ag$_x$O reference electrode, and ferrocene/ferrocenium (Fc/Fc$^+$, 0.42 vs SCE) as an internal reference.

X-ray scattering measurements were carried out using the undulator beam line 12-ID at the Advanced Photon Source (APS), Argonne National Laboratory. The X-ray scattering instrument utilized a double-crystal Si(111) monochromator and a two-dimensional mosaic CCD detector.[80] The X-ray wavelength was set at $\lambda = 0.62$ Å, and the sample to detector distance was adjusted to achieve scattering measured across the 0 Å$^{-1} < q < 0.1$ Å^{-1} region, where $q = (4\pi/\lambda)\sin\theta$, λ is the X-ray scattering wavelength and 2θ is the scattering angle. Glass capillaries (0.2 mm diameter) were used as sample containers. All samples were filtered through 200 nm PTFE filters (Whatman) prior to the measurement. The scattering intensity was averaged over three measurements, after which the solvent scattering was systematically measured and subtracted from the sample spectrum.

Femtosecond transient absorption measurements were obtained using an instrument outfitted with a CCD array detector for the collection of spectral data at multiple delay times following photoexcitation of the

(73) Ballester, P.; Costa, A.; Castilla, A. M.; Deya, P. M.; Frontera, A.; Gomila, R. M.; Hunter, C. A. *Chem.−Eur. J.* **2005**, *11*, 2196−2206.
(74) Ogawa, K.; Kobuke, Y. *J. Photochem. Photobiol., C* **2006**, *7*, 1−16.
(75) Nakagawa, H.; Ogawa, K.; Satake, A.; Kobuke, Y. *Chem. Commun. (Cambridge)* **2006**, 1560−1562.
(76) Hajjaj, F.; Yoon, Z. S.; Yoon, M.-C.; Park, J.; Satake, A.; Kim, D.; Kobuke, Y. *J. Am. Chem. Soc.* **2006**, *128*, 4612−4623.
(77) Furutsu, D.; Satake, A.; Kobuke, Y. *Inorg. Chem.* **2005**, *44*, 4460−4462.
(78) Hunter, C. A.; Meah, M. N.; Sanders, J. K. M. *J. Am. Chem. Soc.* **1990**, *112*, 5773−5780.
(79) Bampos, N.; Marvaud, V.; Sanders, J. K. M. *Chem.−Eur. J.* **1998**, *4*, 335−343.
(80) Seifert, S.; Winans, R. E.; Tiede, D. M.; Thiyagarajan, P. *J. Appl. Crystallogr.* **2002**, *33*, 782−784.

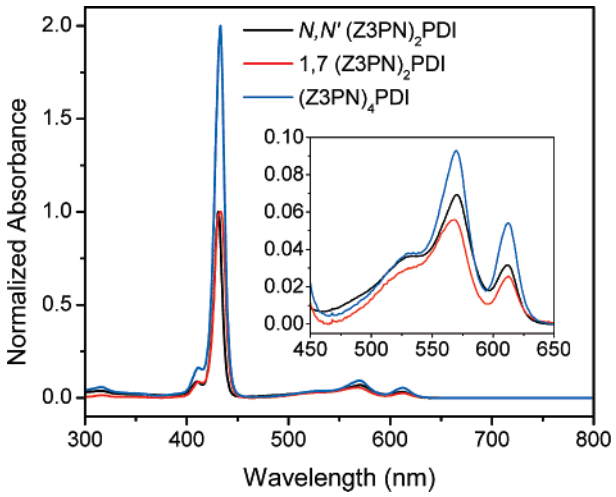

Figure 2. Ground-state electronic absorption spectra of the indicated compounds in toluene with 1% pyridine (v:v). (Inset) Expansion of spectra between 450 and 650 nm.

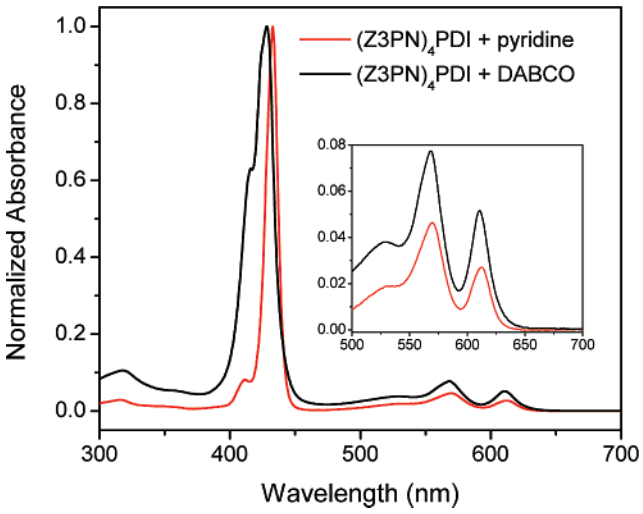

Figure 3. Comparison of the ground-state electronic absorption spectra of $(Z3PN)_4PDI$ with 1% pyridine and with 2 equiv of DABCO in dry toluene. (Inset) Expansion of spectra between 500 and 650 nm.

sample.[81] The total instrument response for the pump−probe experiments was 150 fs. Typically 5 s of averaging was used to obtain the transient spectrum at a given delay time. Cuvettes with a 2-mm path length were used, and the samples were irradiated with 1.0 μJ/pulse focused to a 200-μm spot. The optical density was kept between 0.2 and 0.4 at $\lambda_{ex.}$ Analysis of the kinetic data was performed at multiple wavelengths using a Levenberg−Marquardt nonlinear least-squares fit to a general sum-of-exponentials function with an added Gaussian instrument response function.

Results and Discussion

Donor−Acceptor Building Blocks. The featured compound, $(Z3PN)_4PDI$, was synthesized from 1,7-dibromoperylene-3,4:9,10-tetracarboxydianhydride[15] via sequential imide condensation and Stille cross-coupling reactions with 20-(*p*-aminophenyl)-5,10,15-tripentylporphyrin[81] and zinc 20-(*p*-tri(*n*-butyl)tinphenyl)-5,10,15-tripentylporphyrin, respectively. Metalation of the free-base *N*,*N*′-porphyrins using zinc acetate in $CHCl_3$/MeOH resulted in the final product, $(Z3PN)_4PDI$. Model compounds, *N*,*N*′-$(Z3PN)_2PDI$ and 1,7-$(Z3PN)_2PDI$, were synthesized to independently study electron-transfer pathways through the imide and 1,7-positions. The syntheses for both models were analogous to that of $(Z3PN)_4PDI$, where 4-tributyltintoluene[82] and *p*-toluidine were substituted for zinc 20-(*p*-tri(*n*-butyl)-tinphenyl)-5,10,15-tripentylporphyrin and 20-(*p*-aminophenyl)-5,10,15-tripentylporphyrin to yield *N*,*N*′-$(Z3PN)_2PDI$ and 1,7-$(Z3PN)_2PDI$, respectively. Additional model compounds, zinc 5,10,15,20-tetra(*n*-pentyl)porphyrin (Z4PN)[83] and *N*,*N*′-bis(cyclohexyl)-1,7-diphenylperylene-3,4:9,10-bis(dicarboximide) (1,7-$(Ph)_2PDI$),[84] serve as references for the individual component chromophores.

The ground-state absorption spectrum of $(Z3PN)_4PDI$ in toluene with 1% pyridine (py) at room temperature is compared with those of model compounds *N*,*N*′-$(Z3PN)_2PDI$ and 1,7-$(Z3PN)_2PDI$ in Figure 2. Apart from differences in absorbance due to different Z3PN/PDI ratios, the spectra of the two model systems are almost identical to that of $(Z3PN)_4PDI$. The spectra are indicative of pyridine ligation to each zinc atom with porphyrin Soret bands appearing at 433 nm, porphyrin Q bands at 538, 573, and 615 nm,[56] and additional absorbance between 470 and 590 nm due to the PDI core. As in $(Z3PN\text{-}py)_4PDI$, the spectra of the model compounds between 460 and 665 nm are dominated by porphyrin absorption bands, due to the 2:1 ratio of Z3PN to PDI. The spectra of $(Z3PN\text{-}py)_4PDI$, *N*,*N*′-$(Z3PN\text{-}py)_2PDI$ and 1,7-$(Z3PN\text{-}py)_2PDI$ can be approximately reconstructed using a weighted sum of the component Z3PN and PDI absorptions, which indicates weak ground-state electronic coupling between the chromophores.[85] Steady-state fluorescence from $(Z3PN\text{-}py)_4PDI$, *N*,*N*′-$(Z3PN\text{-}py)_2PDI$, and 1,7-$(Z3PN\text{-}py)_2PDI$ is almost completely quenched ($\phi_F < 0.001$), indicating that efficient photoinduced electron transfer occurs in these systems (see below).

Supramolecular Assemblies. The ground-state absorption spectrum of $(Z3PN)_4PDI$ in dry toluene with two equivalents of DABCO changes significantly, relative to that of $(Z3PN\text{-}py)_4PDI$ in toluene, Figure 3. The $S_0 \rightarrow S_2$ transition of Z3PN in monomeric $(Z3PN\text{-}py)_4PDI$ occurs at 433 nm, which is typical of amine-ligated Zn porphyrins,[31,86] while replacement of pyridine by DABCO blue shifts this transition to 428 nm. It is well-known that cofacial porphyrin dimers show exciton coupling between the two chromophores as evidenced by blue-shifting of the porphyrin Soret bands.[71,73] The porphyrin Q bands at 538, 570, and 613 nm are perturbed to a lesser extent relative to those of $(Z3PN\text{-}py)_4PDI$. The contribution of PDI to the ground-state spectrum is seen as a shoulder at 525 nm in $(Z3PN\text{-}py)_4PDI$, Figure 3. For $(Z3PN)_4PDI$ with 2 equiv of DABCO the 525 nm feature intensifies. Cofacial dimers and higher aggregates of PDI, in which the transition dipole moments are parallel, show an enhanced (0,1) vibronic band relative to the (0,0) band.[15,32,87−89] Overall, these spectral changes are consis-

(81) Kelley, R. F.; Tauber, M. J.; Wasielewski, M. R. *J. Am. Chem. Soc.* **2006**, *128*, 4779−4791.
(82) Justicia, J.; Oltra, J. E.; Cuerva, J. M. *J. Org. Chem.* **2004**, *69*, 5803−5806.
(83) Lindsey, J. S.; Schreiman, I. C.; Hsu, H. C.; Kearney, P. C.; Marguerettaz, A. M. *J. Org. Chem.* **1987**, *52*, 827−836.
(84) Chao, C.; Leung, M.; Su, Y.; Chiu, K.; Lin, T.; Shieh, S.; Lin, S. *J. Org. Chem.* **2005**, *70*, 4323−4331.
(85) Greenfield, S. R.; Svec, W. A.; Gosztola, D.; Wasielewski, M. R. *J. Am. Chem. Soc.* **1996**, *118*, 6767−6777.
(86) Nappa, M.; Valentine, J. S. *J. Am. Chem. Soc.* **1978**, *100*, 5075−5080.
(87) Langhals, H.; Ismael, R. *Eur. J. Org. Chem.* **1998**, 1915−1917.
(88) Li, A. D. Q.; Wang, W.; Wang, L.-Q. *Chem.−Eur. J.* **2003**, *9*, 4594−4601.

tent with self-association of at least two $(Z3PN)_4PDI$ molecules to form $[(Z3PN)_4PDI]_2-DABCO_4$ but do not provide information about the possible formation of higher aggregates or structural information about these aggregates.

In order to determine the stability of $[(Z3PN)_4PDI]_2-DABCO_4$ in solution, a spectrophotometric titration of $(Z3PN)_4PDI$ (4.6×10^{-7} M in chloroform) was conducted, Figure S1. Prior to the addition of DABCO the porphyrin Soret band occurs at 424 nm. Following initial addition of DABCO to the chloroform solution, the absorption band at 424 gives way to a new band centered at 428 nm, which is assigned to the formation of face-to-face porphyrin dimers in which the two porphyrins are bound by a single DABCO.[71] The 428 nm absorption feature increases very little after the addition of 2 equiv of DABCO. However, after the addition of $\sim 10^4$ equiv of DABCO, the band at 428 nm decreases, and a new band at 433 nm appears. This band is due to dissociation of the dimer into two fully ligated, open complexes, $(Z3PN)_4PDI-DABCO_4$. The presence of two isosbestic points in the UV−vis titration data indicates that only three chromophores are present in significant quantity, Figure S2.[71] The equilibrium constants applicable to the three species model are defined as follows:

$$K_{41} = [[(Z3PN)_4PDI] - DABCO_4]/[DABCO]^4[(Z3PN)_4PDI] \quad (1)$$

$$K_{42} = [[(Z3PN)_4PDI]_2 - DABCO_4]/[DABCO]^4[(Z3PN)_4PDI]^2 \quad (2)$$

$$K_{42\leftrightarrow 41} = (K_{41})^2/K_{42} \quad (3)$$

The titration data was fit to a three-chromophore model using multivariate factor analysis (SPECFIT V3.0[90]), Figure S3, to yield the stability constants $K_{41} = (9.7 \pm 3.0) \times 10^{31}$ M^{-5} and $K_{42} = (1.2 \pm 0.2) \times 10^{18}$ M^{-4}. From these stability values, the equilibrium constant for the exchange between the two species was determined to be $K_{42\leftrightarrow 41} = 1.5 \times 10^4$ M^{-3}. These results suggest that the $[(Z3PN)_4PDI]_2-DABCO_4$ dimer is fully formed and stable after the stoichiometric addition of 2 equiv of DABCO to $(Z3PN)_4PDI$ and that a large excess of ligand is required to disrupt the dimer. This knowledge is important for understanding the structure−function relationship of the dimer in solution.

Additional evidence for the formation of a minimal $[(Z3PN)_4PDI]_2-DABCO_4$ structural unit upon addition of two equivalents of DABCO to a solution of $(Z3PN)_4PDI$ is provided by its ^1H NMR spectrum in $CDCl_3$ (not shown). Unfortunately, the ^1H NMR signals of $[(Z3PN)_4PDI]_2-DABCO_4$ in toluene-d_8 are severely broadened, and its UV−vis spectrum is inconclusive regarding both the size and detailed structure of the aggregate. The ^1H NMR resonances of $(Z3PN)_4PDI$ in $CDCl_3$ are broad at room temperature, but the aggregated species exhibits a signal centered around −4.75 ppm, characteristic of DABCO sandwiched between two metalloporphyrins.[78] The absence of signals around 3 and −3 ppm (characteristic of free DABCO and DABCO coordinated to a single zinc porphyrin, respectively) indicates that all of the DABCO ligands in solution reside between two Z3PN moieties. $[(Z3PN)_4PDI]_2-DABCO_4$ also shows resonances at 9.6 ppm, due to the porphyrin β-protons. The cofacial proximity of the two porphyrin π-systems in this assembly causes these signals to experience upfield ring-current-induced chemical shifts relative to the corresponding signals in the monomeric $(Z3PN\text{-}py)_4PDI$ complexes. Methodology other than conventional spectroscopy must be used to elucidate these structures in toluene.

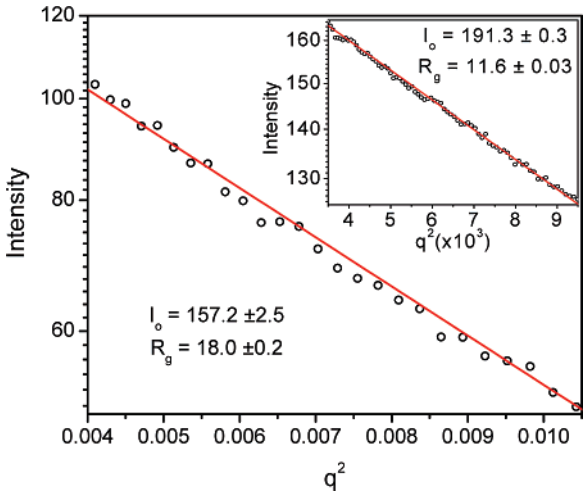

Figure 4. Small-angle X-ray scattering data for $((Z3PN)_4PDI)_2-DABCO_4$ in toluene (2×10^{-4} M) solution. (Inset) SAXS data for $(Z3PN)_4PDI$ in wet toluene (7×10^{-4} M) solution. Guinier fits to the data are also shown.

The structure of $[(Z3PN)_4PDI]_2-DABCO_4$ in toluene was determined by performing small-angle X-ray scattering (SAXS) measurements on $(2-6) \times 10^{-4}$ M samples, see Supporting Information for details. Comparable data in $CHCl_3$ cannot be obtained due to the strong absorption of X-rays by the Cl atoms of $CHCl_3$. The scattering intensity is a function of the scattering vector q, which is related to the scattering angle 2θ by the relationship $q = [(4\pi/\lambda) \sin\theta]$, where λ is the X-ray wavelength. In the low-resolution scattering region ($q < 0.2$ Å^{-1}), the scattering follows the Guinier relationship, $I(q) = I(0) \exp(-q^2R_g^2/3)$, which is parametrized in terms of the forward scattering amplitude, $I(0)$, and the radius of gyration, R_g.[78,91,92] Guinier plots of $(Z3PN)_4PDI$ in wet toluene (0.1%, to ensure complete disaggregation) and $[(Z3PN)_4PDI]_2-DABCO_4$ in dry toluene are presented in Figure 4. The linearity of the Guinier plot is a measure of the compound dispersity.[92,93] $(Z3PN)_4PDI$ shows an essentially linear Guinier plot over the range 0.004 Å^{-2} < q^2 < 0.010 Å^{-2}. The least-squares fit to the linear data reveals $R_g = 11.6 \pm 0.03$ Å. Similar monodispersity and R_g were observed for a THF solution of $(Z3PN)_4PDI$, Figure S4. UV−vis spectra obtained at the conditions of SAXS measurements (10^{-4} M THF and wet toluene solutions) show spectra typical of disaggregated molecules, indicating that $(Z3PN)_4PDI$ is monomeric in both wet toluene and THF.

$(Z3PN)_4PDI$ in dry toluene with 2 equiv of DABCO shows an essentially linear Guinier plot, Figure 4, in the analogous range of 0.004 Å^{-2} < q^2 < 0.01 Å^{-2} and upward deviation from linearity in the region q^2 < 0.004 Å^{-2}. Linearity over the higher q^2 range indicates that the assemblies formed with the

(89) Rybtchinski, B.; Sinks, L. E.; Wasielewski, M. R. *J. Phys. Chem. A* **2004**, *108*, 7497−7505.
(90) *SPECFIT*, version 3.0.38 ed.; Spectra Software Associates: Marlborough, MA, 2006.
(91) Glatter, O. *Neutron, X-ray and Light Scattering*; Elsevier: Amsterdam, 1991.
(92) Guinier, A.; Fournet, G. *Small Angle Scattering*; Wiley: New York, 1955.
(93) Svergun, D. I.; Koch, M. H. *Rep. Prog. Phys.* **2003**, *66*, 1735−1782.

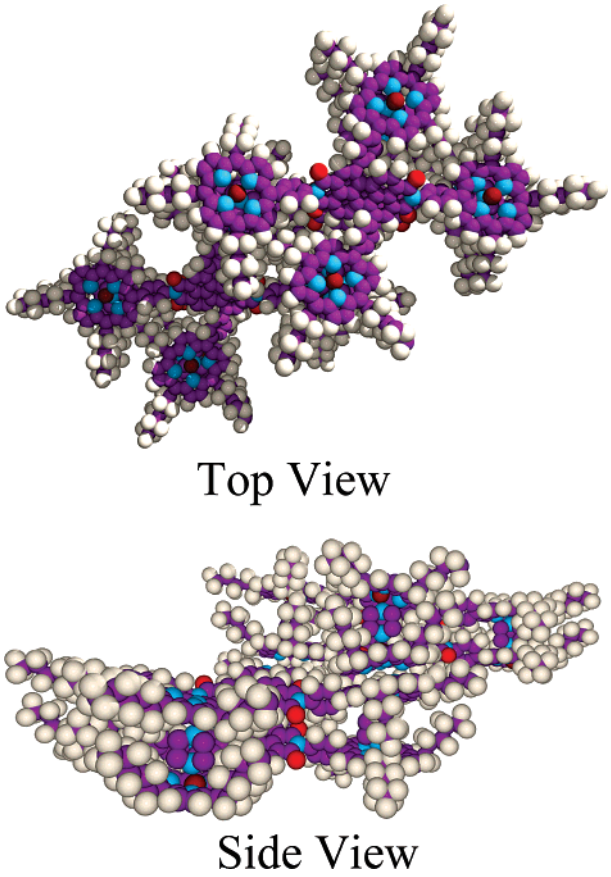

Figure 5. MM+ calculated structure of $[[(Z3PN)_4PDI]_2-DABCO_4]_2$. Views are along the stacking direction (top) and an axis 90° to that direction (side). Simulated $R_g = 17.6$ Å.

addition of DABCO are largely monodisperse. The upward deviation from linear Guinier behavior is characteristic of weakly associating molecular systems[94] and can be attributed to the $\pi-\pi$ interactions characteristic of porphyrin systems.[95] The least-squares fit to the linear data reveals $R_g = 18.0 \pm 0.2$ Å. The Guinier plots also yield the extrapolated intensity at zero scattering angle, $I(0)$, which is proportional to the overall electron density and can be used to estimate the molecular weight of the monodisperse aggregate by comparison to an $I(0)$ value of a monodisperse reference compound of similar structure with known molecular weight.[10,93] By comparing the $I(0)$ obtained from monomeric $(Z3PN)_4PDI$ in wet toluene to that obtained from the higher aggregates of $[(Z3PN)_4PDI]_2-DABCO_4$, we estimate that the assemblies are most likely constructed of two $[(Z3PN)_4PDI]_2-DABCO_4$ complexes. Comparison of the experimentally obtained values for R_g with those generated from a variety of models suggests that the structure of the assembly is a slipped-stacked dimer of $[(Z3PN)_4PDI]_2-DABCO_4$, see Figure 5 (see also Figure S5).

Photoinduced Energy and Electron Transfer. The free energies for photoinduced charge separation (ΔG_{CS}) and charge recombination (ΔG_{CR}) for *N,N′*-$(Z3PN)_2PDI$ and 1,7-$(Z3PN)_2PDI$ were calculated using their experimentally determined redox potentials and the lowest singlet excited-state energy (E_{S1}) of Z3PN, along with computed ionic radii and donor−acceptor distances using the Weller formalism,[96] Table 1 (see Supporting Information for details). The calculated values of ΔG_{CS} predict that photoinduced charge separation should occur readily in both model systems as well as in $(Z3PN)_4PDI$ in toluene.

Table 1. One-Electron Redox Potentials vs SCE (E_{OX}, E_{RED}), Excitation Energies (E_{S1}), and Free Energies[a] of Charge Separation (ΔG_{CS}) and Charge Recombination (ΔG_{CR})

cmpd	E_{OX}	E_{RED}	E_{S1}	ΔG_{CS}	ΔG_{CR}
N,N′-$(Z3PN)_2PDI$	0.62	−0.49	2.04	−0.26	−1.78
1,7-$(Z3PN)_2PDI$	0.62	−0.49	2.04	−0.43	−1.61

[a] Calculated using an expression derived by Weller as described in the text.

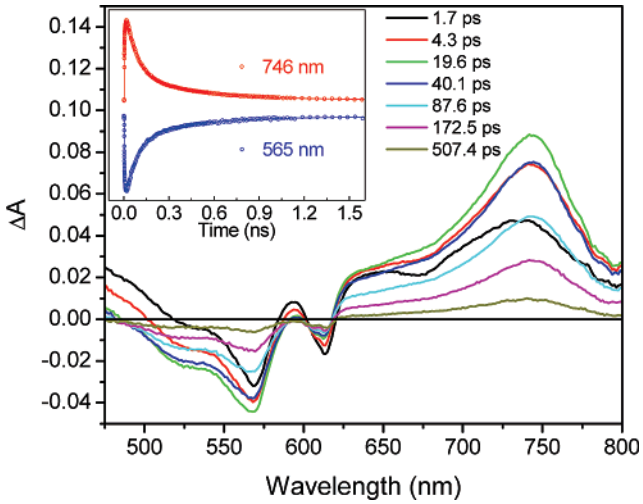

Figure 6. Transient absorption spectra of $(Z3PN)_4PDI$ in toluene with 1% pyridine following excitation with 612 nm, 120 fs laser pulses. (Inset) Transient absorption kinetics for $(Z3PN)_4PDI$ at 565 nm (blue) and 764 nm (red) in toluene with 1% pyridine following excitation with 612 nm, 120 fs laser pulses. Nonlinear least-squares fits to the data are also shown.

Femtosecond transient absorption spectra of $(Z3PN\text{-}py)_4PDI$ in toluene with 1% pyridine (v:v) were obtained using 120 fs, 612 nm pulses, which selectively excite the $S_0 \rightarrow S_1$ transition of Z3PN, Figure 6. The initial spectrum shows $^{1*}Z3PN$ absorption,[60,61] which evolves in time to that of $(Z3PN)_4^{+\bullet}$ [60,61] and $PDI^{-\bullet}$ [97] with absorption features centered around 450 and 744 nm respectively, and ground-state bleaches occurring at 531 and 568 nm for PDI and 614 nm for Z3PN. Transient absorption kinetic traces at 565 and 746 nm, Figure 6 (inset), reveal that the radical ion pair appears with $\tau_{CS} = 5.0 \pm 1.0$ ps and subsequently decays biexponentially with $\tau_{CR} = 81 \pm 6$ ps (60%) and 480 ± 60 ps (40%). Studies on the relevant model systems were performed to clarify the biexponential nature of the charge recombination kinetics within $(Z3PN)_4^{+\bullet}-PDI^{-\bullet}$.

Femtosecond transient absorption measurements on *N,N′*-$(Z3PN\text{-}py)_2PDI$ and 1,7-$(Z3PN\text{-}py)_2PDI$ in toluene with 1% pyridine (v:v) using 120 fs, 612 nm pulses show that the spectral features in the transient spectra of both model compounds, see Figures S6 and S7, are nearly identical to those of $(Z3PN\text{-}py)_4PDI$. The initial spectrum shows features due to $^{1*}Z3PN$, which evolve in time to those of $(Z3PN\text{-}py)_4^{+\bullet}-PDI^{-\bullet}$. Transient absorption kinetic traces at 565 and 745 nm for *N,N′*-$(Z3PN\text{-}py)_2PDI$ reveal that the charge separated state appears with τ_{CS}

(94) Ducruix, A.; Guilloteau, J. P.; Ries-Kautt, M.; Tardieu, A. *J. Cryst. Growth* **1986**, *168*, 28−39.
(95) Tiede, D. M.; Zhang, R.; Chen, L. X.; Yu, L.; Lindsey, J. S. *J. Am. Chem. Soc.* **2004**, *126*, 14054−14062.
(96) Weller, A. *Z. Phys. Chem. (Munich)* **1982**, *133*, 93−98.
(97) Gosztola, D.; Niemczyk, M. P.; Svec, W. A.; Lukas, A. S.; Wasielewski, M. R. *J. Phys. Chem. A* **2000**, *104*, 6545−6551.

$= 9.0 \pm 0.5$ ps and decays with $\tau_{CR} = 1070 \pm 30$ ps, Figure S6 (inset). The corresponding transient absorption kinetics at 570 and 747 nm for 1,7-(Z3PN-py)$_2$PDI reveal that the charge separated state appears with $\tau_{CS} = 10.0 \pm 0.5$ ps and decays with $\tau_{CR} = 77 \pm 3$ ps, Figure S7 (inset).

The transient absorption spectra of (Z3PN-py)$_4$PDI, *N,N′*-(Z3PN-py)$_2$PDI and 1,7-(Z3PN-py)$_2$PDI do not show long-lived absorption changes indicative of the formation of significant yields of either ^{3*}Z3PN or ^{3*}PDI triplet states upon charge recombination. Although the energies of ^{3*}Z3PN and ^{3*}PDI are about 1.7 eV[98] and 1.2 eV,[99] respectively, significant yields of triplet-state formation by either spin−orbit intersystem crossing or by radical pair intersystem crossing do not occur. In the former case, the rates of electron transfer are all far faster than spin−orbit intersystem crossing in either ^{1*}Z3PN and ^{3*}PDI, while in the latter case, the lifetimes of the radical ion pairs are too short and the spin−spin exchange interactions between the radicals are most likely too large for efficient radical pair intersystem crossing.[100]

The transient absorption kinetics for *N,N′*-(Z3PN-py)$_2$PDI and 1,7-(Z3PN-py)$_2$PDI show that the rate constants for CS are comparable, while those for CR differ by a factor of ~12. Electron-transfer rates depend on both the free energy of reaction and the electronic coupling matrix element, V_{DA}, for the process.[15] Considering the free energies of reaction, ΔG_{CS} for 1,7-(Z3PN-py)$_2$PDI (−0.43 eV) is slightly more negative than that for *N,N′*-(Z3PN-py)$_2$PDI (−0.26 eV). This is primarily due to greater Coulombic stabilization in 1,7-(Z3PN-py)$_2$PDI because the ion pair distance is shorter. The total reorganization energy for electron transfer in these systems is due largely to internal nuclear motions with Z3PN and PDI, where $\lambda_I \cong 0.32$ eV,[81] since the solvent contribution, $\lambda_S \cong 0$.[101] In the Marcus model, both CS reactions are close to the peak of the rate vs free energy dependence, so that k_{CS} for 1,7-(Z3PN-py)$_2$PDI should be comparable to that observed for *N,N′*-(Z3PN-py)$_2$PDI, provided that the values of V_{DA} are also comparable. The observed values of k_{CS} for *N,N′*-(Z3PN-py)$_2$PDI and 1,7-(Z3PN-py)$_2$PDI are within experimental error of one another supporting the notion that the values of V_{DA} for the CS reactions are indeed comparable. It is well-known that increased orbital overlap between redox partners leads to a larger value of V_{DA} for electron transfer, which, in turn, produces faster electron-transfer rates.[54,102,103] Electron transfer from ^{1*}Z3PN occurs essentially from the LUMO of Z3PN, which has a large fraction of its π charge density at the β-pyrrole positions of the porphyrin macrocycle. In addition, the LUMO of PDI has considerable electron density at both the carbonyl oxygen atoms and at the 1,6,7,12-carbon atoms,[42] so that the interaction of electron density at the β-pyrrole positions of ^{1*}Z3PN with the LUMO of PDI should be significant irrespective of whether Z3PN is substituted at the *N,N′*- or 1,7-positions of PDI. The interaction of these LUMOs should occur by means of superexchange with orbitals centered on the intervening phenyl joining Z3PN to PDI.

Table 2. Time Constants and Electronic Coupling Matrix Elements for Charge Separation and Charge Recombination in Toluene

cmpd	τ_{CS} (ps)	V_{DA} (cm^{-1})	τ_{CR} (ps)	V_{DA} (cm^{-1})
N,N′-(Z3PN-py)$_2$PDI[a]	9.0 ± 0.5	21	1070 ± 30	250
1,7-(Z3PN-py)$_2$PDI[a]	10.0 ± 0.5	18	77 ± 3	380
(Z3PN-py)$_4$PDI[a]	5.0 ± 1.0		81 ± 6	
			480 ± 60	
[[(Z3PN)$_4$PDI]$_2$−DABCO$_4$]$_2$	3.2 ± 0.2		83 ± 4	
			480 ± 60	

[a] Measured in toluene with 1% pyridine to prevent aggregation

We have calculated the value of V_{DA} using the semi-classical expression of Jortner:[44]

$$k_{ET} = \frac{2\pi}{\hbar}|V_{DA}|^2\sqrt{\frac{1}{4\pi\lambda_S k_B T}}\sum_{n=0}^{\infty}\exp[-S]\frac{S^n}{n!}\exp\left[\frac{-(\Delta G + \lambda_S + n\hbar\omega)^2}{4\lambda_S k_B T}\right] \quad (4)$$

where λ_S and λ_I are respectively the solvent and internal reorganization energies for the electron-transfer reactions, ΔG is either ΔG_{CS} or ΔG_{CR} for the respective charge separation and recombination reactions, ω is the characteristic vibration coupled to the electron-transfer process (usually a C−C stretching frequency of 1500 cm^{-1}), T is the temperature, $S = \lambda_I/\omega$. Details of the parameters and the calculation are given in the Supporting Information. The values of V_{DA} for the charge separation reactions for *N,N′*-(Z3PN-py)$_2$PDI and 1,7-(Z3PN-py)$_2$PDI, Table 2, are comparable and approximately 20 cm^{-1} in accord with our expectations based on the similar values of k_{CS} for the two molecules.

For the CR reactions, the difference in ΔG_{CR} between *N,N′*-(Z3PN-py)$_2$PDI (−1.78 eV) and 1,7-(Z3PN-py)$_2$PDI (−1.61 eV) is also small, but because the CR is in the Marcus inverted region of the rate vs free energy profile, theory predicts that CR for *N,N′*-(Z3PN-py)$_2$PDI should be somewhat slower than that for 1,7-(Z3PN-py)$_2$PDI. In addition to energetic considerations, a slower CR rate for *N,N′*-(Z3PN-py)$_2$PDI is predicted by examining the electronic overlap between the donors and acceptors in the model compounds. As mentioned above, the electron density within the PDI$^{-\bullet}$ differs considerably between the imide nitrogens and the carbon atoms at the 1,7-positions due to the nodal plane, which bisects the two imide nitrogens.[42] In addition, it is well-known that the HOMO of Z3PN$^{+\bullet}$ has substantial charge (and spin) density at the 5,10,15,20-carbon atoms,[58,59] one of which serves as the attachment point to PDI$^{-\bullet}$. Therefore, the electronic coupling matrix element for CR through the 1,7-positions should be considerably larger than that for CR through the imide nitrogen atoms. The calculated value of V_{DA} for 1,7-(Z3PN-py)$_2$PDI is 380 cm^{-1} and is about 50% larger than that for *N,N′*-(Z3PN-py)$_2$PDI, which supports the arguments given above.

The shorter of the two charge recombination lifetimes of (Z3PN-py)$_4$PDI (81 ± 6 ps) is identical within experimental error to that of 1,7-(Z3PN-py)$_2$PDI ($\tau_{CR} = 77 \pm 3$ ps). Since photoexcitation of either the *N,N*-Z3PN or the 1,7-Z3PN chromophores within (Z3PN-py)$_4$PDI is equally probable given their nearly identical electronic absorption spectra, the 81 ps component of CR within (Z3PN)$_4$PDI is most likely due to

(98) Wasielewski, M. R.; Johnson, D. G.; Svec, W. A.; Kersey, K. M.; Minsek, D. W. *J. Am. Chem. Soc.* **1988**, *110*, 7219−7221.
(99) Ford, W. E.; Kamat, P. V. *J. Phys. Chem.* **1987**, *91*, 6373−6380.
(100) Till, U.; Hore, P. J. *Mol. Phys.* **1997**, *90*, 289−296.
(101) Marcus, R. A. *J. Chem. Phys.* **1956**, *24*, 966−978.
(102) del Rosario Benites, M.; Johnson, T. E.; Weghorn, S.; Yu, L.; Rao, P. D.; Diers, J. R.; Yang, S. I.; Kirmaier, C.; Bocian, D. F.; Holten, D.; Lindsey, J. S. *J. Mater. Chem.* **2002**, *12*, 65−80.
(103) Loewe, R. S.; Lammi, R. K.; Diers, J. R.; Kirmaier, C.; Bocian, D. F.; Holten, D.; Lindsey, J. S. *J. Mater. Chem.* **2002**, *12*, 1530−1552.

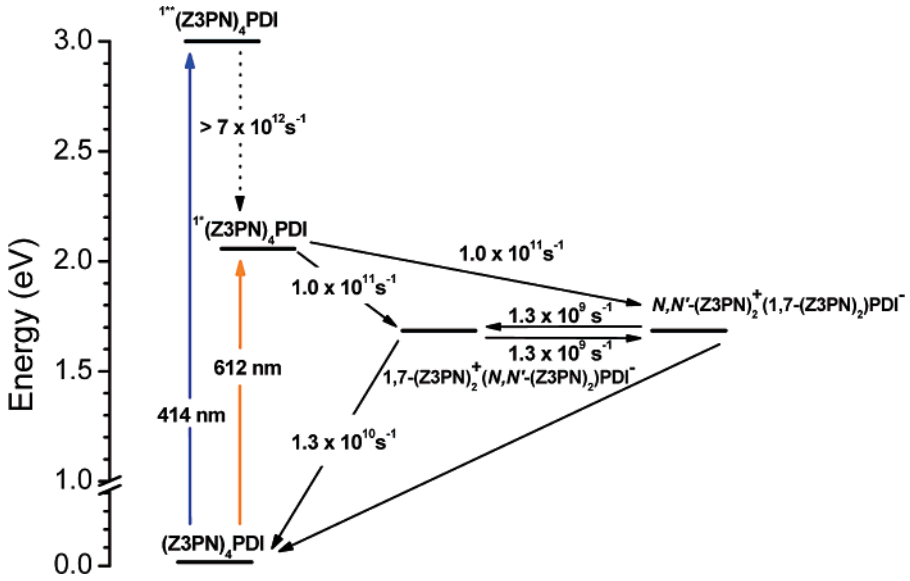

Figure 7. Energy level diagram and time constants for the photoproducts of $(Z3PN)_4PDI$ in toluene with 1% pyridine (v:v).

charge recombination that occurs through the 1,7-positions. The second observed component of charge recombination in (Z3PN-py)$_4$PDI, however, is considerably shorter (480 ± 60 ps) than the charge recombination lifetime observed for *N*,*N*′-(Z3PN-py)$_2$PDI (1070 ± 30 ps). This result can be explained by assuming that statistical formation of *N*,*N*′-(Z3PN-py)$_2^{+\bullet}$−1,7-(Z3PN-py)$_2$PDI$^{-\bullet}$ and *N*,*N*′-(Z3PN-py)$_2$−1,7-(Z3PN-py)$_2^{+\bullet}$-PDI$^{-\bullet}$ occurs, and that CR within these ion pairs is competitive with an equilibrium in which the positive charge is transferred between the *N*,*N*-Z3PN and 1,7-Z3PN chromophores. Using the kinetic scheme shown in Figure 7, the biexponential decay of CR within (Z3PN-py)$_4$PDI can be modeled using equal rate constants of 1.3×10^9 s^{-1} for hole transfer between the *N*,*N*′-Z3PN and 1,7-Z3PN chromophores leading to an equilibrium constant of unity, and therefore $\Delta G = 0$ for this process. Not too surprisingly, this implies that the values of ΔG_{CR} calculated in toluene using the Weller formalism are uncertain by about 0.1 eV.

Femtosecond photoexcitation of (Z3PN-py)$_4$PDI (toluene with 1% pyridine) with 414 nm or 548 nm laser pulses yields transient absorption spectra and time constants identical to those obtained with 612 nm excitation (data not shown). This indicates that both efficient internal conversion from $S_2 \rightarrow S_1$ as well as efficient energy transfer from PDI to Z3PN ($S_1 \rightarrow S_1$) occurs within the 150 fs instrument response. Thus, the excitation energy is efficiently harvested from 400 to 650 nm and funneled into Z3PN, which leads to quantitative charge separation to form the radical ion pair (Z3PN-py)$_2^{+\bullet}$PDI$^{-\bullet}$.

Transient absorption spectra for [[(Z3PN)$_4$PDI]$_2$−DABCO$_4$]$_2$ in toluene were obtained using 120 fs, 612 nm pulses and are shown in Figure 8. The transient spectrum comprises the ground-state bleaches of PDI and Z3PN (occurring at 527 and 569 nm for PDI and 614 nm for Z3PN) as well as the absorbance features of Z3PN$^{+\bullet}$ and PDI$^{-\bullet}$ centered at 450 and 741 nm, respectively. The most significant difference between this spectrum and that of disaggregated (Z3PN-py)$_4$PDI shown in Figure 6 is that the PDI$^{-\bullet}$ absorbance in the spectrum in Figure 8 is significantly broadened and its maximum is slightly blue-shifted by 2 nm. Such broadening and shifting of the PDI$^{-\bullet}$

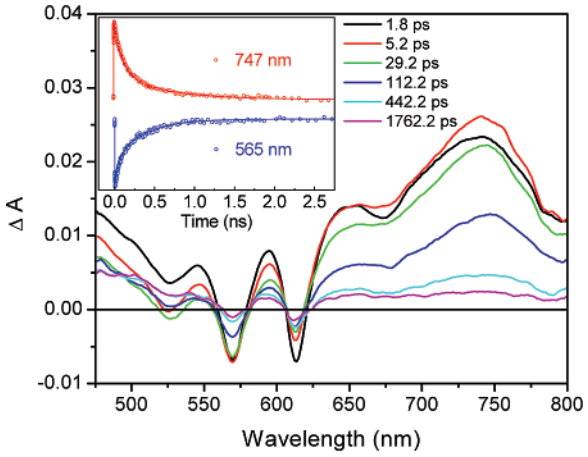

Figure 8. Transient absorption spectra of [[(Z3PN)$_4$PDI]$_2$−DABCO$_4$]$_2$ in toluene following excitation with 612 nm, 120 fs laser pulses. (Inset) Transient absorption kinetics for [[(Z3PN)$_4$PDI]$_2$−DABCO$_4$]$_2$ (blue) at 565 nm and (red) at 747 nm in toluene following excitation with 612 nm, 120 fs laser pulses. Nonlinear least-squares fits to the data are also shown.

spectrum is consistent with a cofacial geometry of π−π stacked PDI chromophores.[15,89] Representative transient kinetics at 565 and 745 nm, Figure 8 (inset), reveal that the radical ion pair appears with $\tau_{CS} = 3.2 \pm 0.2$ ps and decays biexponentially with $\tau_{CR} = 83 \pm 4$ and 480 ± 60 ps, see Table 2.

These data show that charge separation within [[(Z3PN)$_4$PDI]$_2$−DABCO$_4$]$_2$ occurs 1.5 times faster than that in (Z3PN-py)$_4$PDI, while charge recombination in both systems occurs with the same biexponential time constants. Based on the SAXS data, dimerization of [(Z3PN)$_4$PDI]$_2$−DABCO$_4$ in toluene to form [[(Z3PN)$_4$PDI]$_2$−DABCO$_4$]$_2$ results from pairwise π−π interactions between the *N*,*N*′-(Z3PN) of one [(Z3PN)$_4$PDI]$_2$−DABCO$_4$ and the 1,7-(Z3PN) of another [(Z3PN)$_4$PDI]$_2$−DABCO$_4$, Figure 5. The small increase in the charge separation rate constant upon formation of [[(Z3PN)$_4$PDI]$_2$−DABCO$_4$]$_2$ may result from small changes in free energy for charge separation due to the close association of the PDI molecules within each [(Z3PN)$_4$PDI]$_2$−DABCO$_4$ within the dimer.

Since the time constants for biexponential charge recombination in $[[(Z3PN)_4PDI]_2-DABCO_4]_2$ are the same within experimental error as those observed for the $(Z3PN\text{-}py)_4PDI$, it is likely that the charge recombination dynamics within $[[(Z3PN)_4PDI]_2-DABCO_4]_2$ are dominated by the same equilibrium hole transfer between *N*,*N*′-(Z3PN) and 1,7-(Z3PN) that occurs within $(Z3PN\text{-}py)_4PDI$. In $[[(Z3PN)_4PDI]_2-DABCO_4]_2$ there is an additional hole migration pathway—the through-space pathway from *N*,*N*′-(Z3PN) to 1,7-(Z3PN) between the two dimers, which is characterized by shorter distance between the porphyrins. The geometry optimized models reveal center-to-center distances between π-stacking porphyrins of only 3.9 Å. The same models reveal distances between the analogous porphyrins in the covalent system to be 13.8 Å. Unfortunately, the transient absorption spectral features due to $Z3PN^{+\bullet}$ within $[[(Z3PN)_4PDI]_2-DABCO_4]_2$ do not show conclusive evidence for hole hopping between the Z3PN molecules that are bound either by DABCO or by noncovalent interactions, even though the spectra are consistent with electron hopping between adjacent PDI molecules. If the hole-hopping rates between the stacked Z3PN molecules in $[[(Z3PN)_4PDI]_2-DABCO_4]_2$ are very fast, the charge recombination kinetics we observe should still be limited by the intrinsic rates observed in the $(Z3PN\text{-}py)_4PDI$ monomer. Electron−nuclear double resonance (ENDOR) experiments on a single $Z3PN^{+\bullet}$ produced within the $[[(Z3PN)_4PDI]_2-DABCO_4]_2$ assembly are capable of determining whether hole hopping in this system occurs with rate constants $>10^7$ s^{-1},[104] and will be reported in a future publication.

(104) Tauber, M. J.; Kelley, R. F.; Giaimo, J. M.; Rybtchinski, B.; Wasielewski, M. R. *J. Am. Chem. Soc.* **2006**, *128*, 1782−1783.

Conclusions

Directional charge transport in tailored, self-assembling molecular materials is essential for the development of organic photovoltaics. The studies reported here reveal that it is possible to rapidly transfer charge between adjacent sites in an ordered array of identical chromophores, as a result of structural and electronic asymmetry in the array at both the molecular and supramolecular level. This asymmetry creates different electronic couplings and Coulombic interactions between the photoinduced charges, depending on their location on the array, making one pathway for charge recombination favorable over the other. This allows control over charge recombination directionality and may prove to be an important design principle for the development of new supramolecular materials for organic photovoltaics.

Acknowledgment. This research was supported by the Office of Naval Research under Grant No. N00014-05-1-0021. We thank Drs. Xiaobing Zuo and David M. Tiede (Chemistry Division, Argonne National Laboratory) for assistance with SAXS experiments. Use of the Advanced Photon Source was supported by the U.S. Department of Energy, Office of Science, Office of Basic Energy Sciences, under Contract No. W-31-109-ENG-38.

Supporting Information Available: Experimental details, including the synthesis and characterization of the molecules, SAXS, modeling, and transient absorption. This material is available free of charge via the Internet at http://pubs.acs.org.

JA0664741